HIF-3α-Induced miR-630 Expression Promotes Cancer Hallmarks in Cervical Cancer Cells by Forming a Positive Feedback Loop

Qiaohui Gao
Air Force Medical University
Zhenghua Ren
Air Force Medical University
Shengyuan Jiao
Air Force Medical University
Juan Guo
Air Force Medical University
Xia Miao
Air Force Medical University
Jin Wang
Air Force Medical University
Junye Liu (junyeliu@fmmu.edu.cn)
Air Force Medical University

Research Article

Keywords: Hypoxia, HIF3A, miR-630, HeLa cell, cancer hallmarks

Posted Date: October 13th, 2021

DOI: https://doi.org/10.21203/rs.3.rs-900566/v1

Abstract

Background Hypoxia has crucial functions in cervical cancer development and metastasis by inducing the level of numerous genes, including microRNA genes. But we know little about how the hypoxia factors and microRNAs orchestrate to regulate hallmarks of cervical cancer cells.

Methods We used RNA sequencing (RNA-seq) and chromatin immunoprecipitation sequencing experiments (ChIP-seq) to investigate the targets of HIF-3α or miR-630. ChIP-qPCR and RT-qPCR were used to validate the sequencing results of ChIP-seq and RNA-seq. Cellular, molecular and radiation experiments were used to explore the functions of miR-630.

Results Here, we show that hypoxia-induced overexpression HIF-3α increased the expression of dozens of miRNAs, including miR-630. Further experiment showed the activation of miR-630 was induced by hypoxia treatment. We showed that hypoxia induces expression of HIF-3α to activate miR-630 expression by directly binding to its promoter. Meanwhile, miR-630 positively regulates HIF-1α expression, but represses HIF-1α. Stable overexpression of miR-630 in HeLa cells promotes cancer hallmarks, including radioresistance, inhibition of apoptosis, increased migration and invasion, and EMT-mediated metastasis. Stable inhibition of miR-630 showed opposite features.

Conclusion Taken together, our findings implicate a novel hypoxia-induced HIF3a-miR-630 regulatory feedback loop contributing to metastasis and progression of cervical cancer cells, and suggest HIF3a and miR630 might be applied as a potential biomarker and therapeutic target for cervical cancer.

Background

Cervical carcinoma (CC) is a common gynecological cancer that seriously threatens women's health [1]. A third of patients with cervical cancer occur tumor recurrence and metastasis in two years after radiotherapy [2]. Extrinsic abnormalities tumor microenvironment, particularly tumor hypoxia reduces the efficacy of radiotherapy and shortens survival time and increases recurrences [3]. Hypoxia-inducible factor (HIF) is a transcriptional activator of various genes related to cellular adaptive responses to hypoxia. To date, three HIF family members have been identified in mammals (HIF-1α, HIF-2α, and HIF-3α). HIF1A targeted genes are most significantly associated with metabolism of carbohydrates, diabetes pathways, pathways in cancer, integration of energy metabolism [4]. Up-regulation of HIF3A can accelerate the progression of ovarian cancer and promote metastatic phenotypes in pancreatic cancer [5]. However, much less is known how HIF3A functions in cervical cancer.

Recent studies demonstrate that miRNAs play an important role in modulating the process of EMT [6]. For example, miR-27b could induce EMT and promote cervical cancer metastasis [7]. Our previous data indicated that a specific miRNA signature including miR-630, miR-1246, miR-1290 and miR-3138 could promote radioresistance of human cervical cancer cells [8]. MiR-630, identified from the miRNA cluster at chromosome 15q24.1, has been demonstrated to be deregulated and involved in several human

malignancies [9]. Further study is needed to clarify the mechanisms of miR-630 on cancer development and progression.

In this study, we investigated the regulatory loop among HIFs and miR-630 to identify their functions in cervical cancer progression. Firstly, we confirmed that miR-630 is upregulated by HIF3A but not by HIF1A in cervical cancer cells. Secondly, we explored the relationship between hypoxia and radiation through the expression of miR-630. Thirdly, HIF1A can be regulated by HIF3A and miR-630 could increase HIF3A expression but repress HIF1A expression. We proved the role of HIF3A-miR630 loop in regulating radioresistance and metastasis, providing new ideas for individualized treatment of cervical cancer.

Methods

Cell culture

HeLa cells were purchased from the Institute of Biochemistry and Cell Biology, Chinese Academy of Sciences in 2018. HeLa cell was maintained as a monolayer in Dulbecco's modified Eagle's medium (DMEM, Invitrogen, Carlsbad, CA) supplemented with 10% fetal bovine serum (FBS,Sijiqing Biological Engineering Materials Co., Hangzhou, China) at 37°C in the presence of 5% CO_2-balanced air. The other three stable transformants was maintained as a monolayer in DMEM with 10% FBS and 2ug/ ml puromycin (Sigma, German).

Hypoxia

To induce hypoxia, HeLa cell was rendered in a chamber with a gas mixture of 1% O_2 and 5% CO_2-balanced N_2 at 37°C. The level of oxygen in the chamber was verified using a gas monitor (SKC, Inc., Eighty Four, PA). To mimic hypoxia using chemicals, cells were cultured under 20% oxygen in the presence or absence of 100 μM $CoCl_2$ for a specified time period.

Plasmid Construct And Transfection

Full-length human *HIF3A* cDNA was cloned into a Pcmv-ORF-flag-his expression vector and *HIF1A* was cloned into a pBabe-puro-HA expression vector (TranSheepBio, Shanghai, China). Transfection was performed with lipofectamine 2000 (Invitrogen, Carlsbad, CA, USA) 24 h after cell seeding. Lentiviral constructs containing up-regulating miR-630 (LV-hsa-mir-630), inhibiting miR-630 (LV-hsa-mir-630-inhibitor) and the negative control lenti-vector (LV-Negative Control) were designed and provided by Genechem Inc. (Shanghai, China). 60–70% confluent HeLa cell was infected with three lenti-virus at multiplicity of infection (MOI) of 10 with enhanced infection solution (ENI.S) according to the manufacturer's protocol. 10 hours post-infection, viruses were replaced by complete DMEM and 48 hours post-infection, three stably infected cells (LV-hsa-mir-630, LV-hsa-mir-630-inhibitor, LV-Negative Control)

were selected by DMEM with 2 μg/ ml puromycin (Sigma, German). The expression level of miR-630 in the stable transformants were identified by qRT-PCR.

Quantitative Real-time Pcr

The expression level of miR-630 in the cells were determined using real-time PCR. Total RNA was extracted using Trizol reagent (Invitrogen, Carlsbad, CA) and reverse transcription was performed according to manufacturer's instructions (638315, Clontech Laboratories, Inc. A Takara Bio company, USA). qRT-PCR was performed to determine the expression level of miR-630 using the exact sequences (U to T) of miR-630 as the forward primer and the unique q-PCR primer from the cDNA Synthesis Kit as the reverse primer. U6 was used as an internal control, and each plate contains one cDNA sample for each primer as a correct sample. Primers were shown in Table S1.

Transwell Chamber Assay

The invasive ability of cells was performed in 24-well transwell chambers (Corning, NY). The polycarbonate filters containing 8-μm pores were coated on ice with 80 μl of Matrigel (Sigma-Aldrich) at 5 mg/L. After blocking with 1% BSA for 1h at 37°C the cells (5 x 10^5/mL) were suspended in serum-free culture medium, 100μl were added to the upper compartments of chamber. In each lower chamber, 500μl of medium (10% FBS) was added. After 24h incubation the cells from the upper compartment were removed, and the cells on the lower surface were fixed in ethanol and stained with hematoxylin-eosin. Cells on the lower surface were quantified in 10 random microscopic fields per filter at a magnification of x200 (DMI4000B, LEICA, Germany).

Western Blot Analysis

Western blot analysis

When 80% confluence in 25 cm^2 flasks (Nunc, Roskilde, Denmark) was reached, the cells were lysed with RIPA lysis buffer (Beyotime, Shanghai, China) on ice, and then centrifuged at 12000 rpm for 20 min. Supernatants were collected and protein was determined using Bicinchoninic acid (BCA) kit (Boster, Wuhan, China). The extracts (20 μg per lane) were fractionated by 10% SDS-PAGE and then transferred onto PVDF membranes (0.45 μm; Millipore, Bedford, MA). After blocking with TBST buffer (20 mM Tris-buffered saline and 0.1% Tween-20) containing 5% non-fat milk for 1h at 25℃, the membranes were incubated with primary antibodies against E-cadherin□N-cadherin (1:5000,Epitomics, USA), Cytokeratin (1:400, Boster, China), EP300 (1:1000, Abnova, USA) and β-actin (1:5000, Cmctag, USA) overnight at 4°C. Membranes were washed three times x 5 min with TBST before incubation with horseradish peroxidase–conjugated secondary antibody (1:3000, CST, USA) for 60 min at 25℃. The membranes was exposed by chemiluminescence (Millipore, Billerica, MA), and images were acquired by ChemiDoc XRS (Bio-Rad, Hercules, CA). Semi-quantification of scanned films was performed using Quantity One-4.6.2 (Bio-Rad).

Immunofluorescence

Cells were grown on 24-well m-Slides (NEST Biotechnology Co.LTD. Wuxi, China) and fixed with 4% paraformaldehyde for 30 min at 4°C, followed by treatment with 0.1% Triton for 10 min. The samples were blocked with PBST buffer (0.1% Tween-20) containing 10% goat serum at room temperature for 1 h and incubated with primary antibodies E-cadherin, N-cadherin (1:500, Epitomics, USA), Cytokeratin (1:200, Boster, China), for overnight at 4°C. The cells then washed in PBST and incubated with DyLight 488 and DyLight 594 conjugated secondary antibodies (ZS-Bio) at room temperature in the dark for 1 h. Nuclei were counterstained with DAPI for 5 min. After washing three times, the cells were maintained with 50% glycerin in PBS and observed by laser confocal microsopy (Fluoview FV1000; Olympus, Tokyo, Japan). Photographs were taken through a digital camera (Olympus Fluoview FV1000) attached to the microscope. Ten images (approximately 30 cells per field) were acquired in each group, the quantification of gray value was analyzed with Olympus Fluoview software FV10-ASW 1.7.

Rna-seq Library Construction And Sequencing

5μg of total RNA was used for RNA-seq library preparation. Polyadenylated mRNAs were purified and concentrated with oligo (dT)-conjugated magnetic beads (invitrogen) before directional RNA-seq library preparation. Purified mRNAs were iron fragmented at 95℃ followed by end repair and 5' adaptor ligation. Then reverse transcription was performed with RT primer harboring 3' adaptor sequence and randomized hexamer. PCR products corresponding to 200–500 bps were purified, quantified and stored at -80℃ until sequencing. The libraries were prepared and applied to illumina NextSeq 500 system with 150x2 paired-end type (ABLife Inc., Wuhan, China).

Mirna-seq Library Construction And Sequencing

Total RNA (3μg) was used for small RNA cDNA library preparation with Balancer NGS Library Preparation Kit for small/microRNA (Genome Gen). Briefly, RNAs were ligated to 3' and 5' adaptor sequentially and reverse transcribed to cDNA and then PCR amplified. Whole library was applied to 10% native PAGE gel electrophoresis and bands corresponding to microRNA insertion were cut and eluted. The purified small RNA libraries were quantified and stored at -80℃. The libraries were prepared following the instructions and applied to illumine NextSeq 500 system with 150x2 paired-end type (ABLife Inc., Wuhan, China).

Chromatin Immunoprecipitation (Chip) Library Construction And Sequencing

Total cell extracts were prepared from $2x10^7$ formaldehyde fixed cells resuspended in 1 mL lysis buffer containing 50 mM Tris 7.4, 150 mM NaCl, 2 mM EDTA, 0.1% SDS, 0.5% NP-40 and 0.5% deoxycholate. The suspension was sonicated to generate DNA fragments of 200-500bp, centrifuged for 10 min at

12,000 g, 1000μL cell extracts were incubated with HIF3A antibody (orb101652, Biobyt, China) overnight at 4 ℃. The immunoprecipitates were further incubated with protein A Dynabeads for 3h at 4 ℃. After applying to magnet and removing the supernatants, the beads were sequentially washed with lysis buffer, high-salt buffer (250 mM Tris 7.4, 750 mM NaCl, 10 mM EDTA, 0.1% SDS, 0.5% NP-40 and 0.5 deoxycholate), and PNK buffer (50 mM Tris, 20 mM EGTA and 0.5% NP-40) for two times. The immunoprecipitates were eluted from the beads with elution buffer (50 nM Tris 8.0, 10 mM EDTA and 1% SDS) and reverse cross-linked overnight-incubated at 65 ℃. After sequential RNase A and proteinase K treatment, DNA fragments were purified by phenol extraction and ethanol precipitation. Purified DNA fragments were end-repaired, adenylated, ligated to adaptors and PCR amplified for 12 cycles. The PCR products corresponding to 300–500 bps were gel purified, quantified and stored at -80 ℃. The libraries were prepared and applied to illumina X-Ten system with 150x2 paired-end type by Novogene.

Rna-seq Data Processing And Alignment

Raw reads containing more than 2-N bases were first discarded. Then adaptors and low-quality bases were trimmed from raw sequencing reads using FASTX-Toolkit (Version 0.0.13). The short reads less than 16 nt were also dropped. After that, clean reads were aligned to the GRCh38 genome by TopHat2 [10] allowing 4 mismatches. Uniquely mapped reads were used to calculate reads number and FPKM value (fragments per kilobase of transcript per million fragments mapped) [11] for each gene.

Differentially Expressed Genes Analysis

The R Bioconductor package edgeR [12] was utilized to screen out the differentially expressed genes (DEGs). A false discovery rate < 0.05 and fold change > 2 or < 0.5 were set as the cut-off criteria.

To predict the gene function and calculate the functional category distribution frequency, Gene Ontology (GO) analyses and enriched KEGG pathway were identified using KOBAS 2.0 server [13]. Hypergeometric test and Benjamini-Hochberg FDR controlling procedure were used to define the enrichment of each pathway (corrected p-value < 0.05).

Statistical analysis

All the statistics were expressed as mean ± standard deviation (SD) and processed using SPSS 16.0 statistical software (Chicago, IL). All experiments were performed at least three times independently,and $P < 0.05$ were considered significant.

Results

HIF3α participates in the hypoxia-induced activation of miR-630 transcription

Previous study has demonstrated that the expression pattern of miRNAs was regulated by hypoxia [14]. According to the established work, the hypoxia-inducible factors, including HIF-1α, HIF-2α, and HIF-3α, are regulators of oxygen homeostasis [15]. We selected the well-studied HIF-1α and poorly studied HIF-3α and confirmed their elevated expression level in HeLa cells cultured under hypoxia (Fig. 1A-B). Consistent with previous study [5], HIF-3α expression level was stimulated to a greater degree than that of HIF-1α (Fig. 1A-B). Re-analysis of TCGA cervical cancer revealed their converse expression pattern between normal and tumor samples (Fig. S1A). However, higher expression of HIF-1α and HIF-3α both could shorten the survival time of cervical cancer patients (Fig. S1B), indicating their oncogenic functions.

We then investigated if the expression of miRNAs was also regulated by HIF-3α, as has been reported by HIF-1α. We utilized the HIF-1α or HIF-3α overexpression and vacant HeLa cells to generate miRNA expression profile by miRNA-sEq. Differentially expressed miRNAs (DEmiRs) analysis revealed the up-regulated miRNAs were dominant in both HIF-1α and HIF-3α overexpressed samples (Fig. 1C). Meanwhile, we analyzed expression of miRNAs previously identified by our group that are involved in radioresistance in cervical cancer cells [8]. The expression of miR-630 was increased in both HIF-1α and HIF-3α OE samples, especially the HIF-3α OE samples (Fig. 1D). Except miR-630, miR-137 was significantly up-regulated in HIF-3α overexpressed HeLa cells. MiR-1246 and miR-137 were significantly up-regulated in HIF-1α overexpression cells. However, miR-15b-3p was significantly down-regulated in HIF-1α overexpression cells (Fig. 1D). qRT-PCR also showed that HIF-3α increased the expression level of miR-630, similar with RNA-seq results (Fig. 1E).

We then measured miR-630 expression level in HeLa cells which were cultured under hypoxia for 24h and 48h. We found that miR-630 was upregulated in response to hypoxia. After 24h exposure to hypoxia, HeLa cells then were incubated in normoxia for 24h. We found that the miR-630 level was still higher than control (Fig. 1F). These results show that the activation of miR-630 by hypoxia is fast and long lasting in HeLa cells.

The Cancer Cell Transcriptome Changes Upon Hif-3α Overexpression

To further explore the functions of targets regulated by HIF-3α, we performed HIF-3α overexpression and silence experiments, and utilized transcriptome profiling by RNA-seq for HIF-3α OE and negative control samples in HeLa cells. Sample correlation analysis revealed the global alteration of transcriptome by HIF-3α overexpression (Fig. 2A). We finally obtained a total of 201 DEGs, including 172 up-regulated and 29 down-regulated genes (Fig. 2B and Fig. 2C). GO and KEGG pathway analysis for the up-regulated genes by HIF-3α OE. The up-regulated target genes are enrichment in terms including response to virus, type I interferon-mediated signaling pathway, negative regulation of apoptotic process. Enriched KEGG pathways included hematopoietic cell lineage, TNF signaling pathway, cytokine-cytokine receptor interaction, and transcriptional mis-regulation in cancer (Fig. 2D). These data indicated that HIF-3α can up-regulate the transcriptional level of cancer-related genes, including *ETV1, ETV5, ETV4, CXCL8, HMGA2,*

IL6, DUSP6, ARNT2, PTGS2, SOCS3, CCL5, FOS, JUN, IL6, and *VEGFC* (Fig. 2E). Immune and inflammatory related terms were also significantly enriched (Fig. 2D). HIF-3α overexpression significantly increased RNA level of *HIF1A* (Fig. 2F), indicating HIF-3α positive regulation on *HIF1A* expression.

HIF-3α globally binds to the promoters of miR-630 and HIF1A, and also some other miRNAs, mRNA and lncRNAs

To decipher how HIF-3α regulate the expression of their target genes, we performed ChIP-seq for HIF-3α. After aligning the quality filtered reads to the human genome, we predicted the binding peaks by MACS2 software [16]. We then assessed the reads distribution around the transcription start sites (TSS) of all genes. We observed ChIP-seq tags were obviously enriched in the TSS region of HIF3A (Fig. 3A), suggesting that HIF-3α binds to the promoter region to regulate gene expression. By classifying the HIF3A-bound peaks according to their genomic distribution, about 21 ~ 30% peaks were located at the TSS region of genes (within 2kb to TSS, Fig. 3B). We also found that HIF3A globally bound to the promoters of miRNAs, mRNA, and lncRNAs (Fig. 3C). The percentages of bound miRNAs were 9% and 12% for the first and second replicates of HIF-3α, respectively. We then assessed how HIF-3α regulate gene expression by directly binding to their genomic locus. 41.8% (84) of HIF-3α-regulated DEGs were bound by HIF-3α (Fig. 3D). Among these, miR-630, miR-137 were bound by HIF-3α at the promoter region of their host genes. We showed miR-137 as an example (Fig. 3E). To verify the ChIP-seq results, ChIP-qPCR experiment was conducted for selected miRNAs (Fig. 3F), which confirmed that miR-155, miR-158, miR-95, miR-1290, and miR-137 were directly bound by HIF-3α.

MiR-630 overexpression increases the HIF-3α activation and suppressed HIF-1α activation

Furthermore, miR-630 is an intronic miRNA that uses the same promoter with its host gene *ARIH1*. Sequencing reads carrying the HRE binding motif were enriched in the promoter of the *ARIH1* gene in HIF3A IP ChIP-seq samples (Fig. 4A). This finding was validated by ChIP-qPCR (Fig. 4B). Taken together, these data demonstrated that expression of miR-630 was activated by HIF3A binding to its host gene promoter. Since radiation and hypoxia both induce the expression of miR-630 in cervical cancer cells, we investigated potential relationship between miR-630 and HIFs. By checking the protein level of HIF1A and HIF3A, we found miR-630 could significantly reduce HIF1A expression, but increase HIF3A expression (Fig. 4C-D).

While it is clear that miR-630 can promote cell proliferation and invasion, the associated regulatory mechanism for miR-630 is unclear. We performed RNA-seq for miR-630 knockdown and vacant HeLa cells. A total of 8413 DEGs, of which 5107 were up-regulated and 3306 were down-regulated (Table S2). Functional enrichment analysis among the DEG genes (Fig. 4E) showed that the up-regulated genes entrenched in “transcription, DNA-dependent”, “regulation of transcription, DNA-dependent”, “response to DNA damage stimulus”, “mitotic cell cycle”, and “double-strand break repair via homologous recombination”. The down-regulated genes are enriched in pathways “mRNA metabolic process”, “translation”, and “extracellular matrix organization” (Fig. 4E). We also found that the expression of *ATM* and *ATR* genes, the master of cell cycle checkpoint signaling pathways [17], was upregulated by silencing

miR-630 in HeLa cells (Fig. 4F). RNA-seq data also revealed significant downregulation of *HIF1A* by miR-630 knockdown (Fig. 4G), and upregulation of *HIF-3α* by miR-630 knockdown in HeLa cells (Fig. 4G).

MiR-630 promotes HeLa cell survival and proliferation by its radioresistance activity

To explore the cellular influence of miR-630 on cervical cancer cells, we established cervical cancer HeLa cells with stably overexpressed and inhibited miR-630 level by lentivirus transfection (Fig. 5A). Our previous study showed that radiation induced the expression of miR-630 in cervical cancer cells with a time- and dose-dependent manner [8]. Colony formation assay was used to analyze HeLa cell survival rate in single-dose radiotherapy (0Gy, 4Gy, 8Gy and 10Gy). We found that overexpression of miR-630 attenuated radiotherapy-induced apoptosis of HeLa cells while silencing of miR-630 accelerated radiotherapy-induced apoptosis (Fig. 5B), indicating the radioresistant function of miR-630. To further explore the functions of miR-630, we measured cell proliferation after 6Gy and 8Gy radiotherapy. Overexpression of miR-630 had a positive effect on the proliferation capacity of HeLa cells while silencing of miR-630 resulted in decreased proliferation (Figs. 5C and D). Taken together, these data demonstrated that miR-630 enhanced the radioresistance and increased proliferation of HeLa cells.

MiR-630 inhibits both spontaneous and radiation-induced apoptosis of HeLa cells

We then investigated the effect of miR-630 on apoptosis level in cervical cancer HeLa cells by using Flow cytometry analysis. We found that overexpression of miR-630 inhibited spontaneous apoptosis of HeLa cells ($P < 0.05$), however, silencing of miR-630 had no influence on spontaneous apoptosis of HeLa cells ($P > 0.05$) (Fig. 5E). When HeLa cells were then subsequently treated with 6Gy and 8Gy doses of radiotherapy, we found that overexpression of miR-630 suppressed the apoptosis of HeLa cells in vitro ($P < 0.05$) (Fig. 5F and 5G). Silencing of miR-630 promoted the apoptosis of HeLa cells in vitro ($P < 0.05$) (Fig. 5F and 5G). Subsequently, we detected apoptosis proteins such as BCL2, BAX, Caspase 3, Caspase 7, and Caspase 9 in 6Gy HeLa cells. We found that expression of BCL-2 increased while BAX decreased (Fig. 5H). Caspase 3, Caspase 7, and Caspase 9 were all significantly decreased under miR-630 overexpression condition (Fig. 5I). Taken together, these data demonstrated that miR-630 inhibited spontaneous and radiation-induced apoptosis of HeLa cells in vitro.

Mir-630 Enhances Hela Cell Migration And Invasion In Vitro

To determine the role of miR630 in regulating migration and invasion of HeLa cells, we used wound healing assay and transwell chamber assay (Fig. 6A and C, Fig. S2A). Wound healing assay indicated that overexpression of miR-630 enhanced HeLa cell migration ($P < 0.05$), while the relative migration distance of miR-630 inhibited cells was significantly decreased ($P < 0.05$) (Fig. 6A and Fig. S2A). Furthermore, the transwell assay showed that invasion rate was significantly increased ($P < 0.05$) (Fig. 6B-C). In contrast, silenced miR630 significantly inhibited the invasion ($P < 0.05$) (Fig. 6C). Real time cellular analysis (RTCA) revealed the significantly higher motility of HeLa cells with miR-630 overexpression (Fig.

S2B, P = 0, K-S test). In conclusion, overexpression of miR-630 significantly enhanced the migration and invasion capacity of cervical cancer *in vitro*.

Mir-630 Could Promote Hela Cell Metastasis And Emt

From the above RNA-seq results under miR-630 inhibition, we noted that the EMT-related transcription factors (SNAI1, ZEB1, ZEB2) were up-regulated, while TWIST1 and SMAI2 were down-regulated (Fig. 6D). We also found *EP300*, a metastasis suppressor gene and a known direct target of miR-630 [18], was one of the miR-630-inhibition up-regulated DEG (Fig. 6D). *EP300* was up-regulated upon silencing of miR-630 and down-regulated upon overexpression of miR-630 (Fig. 6E). These results suggested miR-630 may promote EMT in HeLa cells. To further confirm miR-630 functions in EMT, we performed cellular morphological change experiment in HeLa cells. We found that miR-630-induced morphological changes in HeLa cells consistent with EMT treatment (Fig. 6F). We checked the expression change of canonical EMT markers, including E-cadherin and N-cadherin. We found that overexpression of miR-630 increased expression of N-cadherin, and decreased E-cadherin compared with the control group ($P < 0.05$) (Fig. 6G-H). Above data suggest that miR-630 can promote HeLa metastasis by EMT in cervical cancer cells. The induction of HIF-3α under hypoxia increase transcription of miR-630, and miR-630 overexpression also has positive impact on HIF-3α expression. In conclusion, we can describe a positive regulatory loop between miR630 and HIF-3α. Our results also showed that overexpression of miR-630 could significantly increase the proliferation, invasion, metastasis, and EMT of HeLa cells, reduce the apoptosis (Fig. 6I).

Discussion

In our studies, we described a regulatory loop between HIF3A and miR-630 (Fig. 6I). Overexpression of miR630 increases the expression of HIF3A, but decreases the expression of HIF1A. Overexpression of HIF3 increases the expression of miR630. The cellular functions of miR-630 were extensively investigated to support its carcinogenic function. We also found HIF3A cooperates the expression of cancer cell transcriptome. These results demonstrated the novel HIF3A-miR630 axis to promote HeLa cell development at multiple aspects. Several miRNAs has been demonstrated in radioresistance, such as miRNA-668 in breast cancer [19] and miR-125 in cervical cancer cell [20]. Our previous study demonstrated that overexpression of miR-630 in HeLa cells results in radioresistance [8]. In this study, we showed that overexpression of miR-630 significantly promoted the migration, invasion, and EMT-mediated metastasis of HeLa cells, and inhibited the apoptosis. Several studies have demonstrated the bidirectional functions of miR-630. One side, miR-630 has a tumor suppressor role, inhibiting tumor progression [21]. Conversely, miR-630 also act as an oncogene, promoting tumor progression and consequently resulting in poor prognosis [22]. Specially, Yuan-Yuan Lyu reported that MiR-630 acts as a tumor suppressor in cervical cancer and inhibits EMT in cervical cancer [23]. We suspected that one miRNA may target a set of mRNAs, might affect radiosensitivity [24].

The mechanisms of HIF1A have been extensively studied in multiple cancer types [25]. However, the functional studies focusing on HIF-3α were only emerged in recent years. It was generally thought that HIF-3α plays a negative role in the hypoxic induction of gene expression by competing with HIF-1α and HIF-2α in binding to transcriptional elements in target genes during hypoxia [26]. The expression of HIF-3α in zebrafish is oxygen-dependent and acts as a transcription activator [27]. In our results, HIF-3α can be significantly induced by hypoxia and increase the expression of multiple miRNAs, consistent with the master regulator of hypoxia in microRNA biogenesis and activity [14]. We found HIF-3α activates miRNA expression by directly binding to their promoter region. Transcriptome sequencing suggested the transcriptional activation role of HIF-3α. Up-regulated of HIF-3α can greatly activate the cancer development related genes. Bioinformatics analysis of genes indicated that HIF-3α and HIF-1α regulate the common biological processesc.

Next, we focused on a HIF-3α activated miRNA, miR-630, to explore its cellular function. MiR-630 was upregulated under hypoxia and increased tumor growth and metastasis by delivered into ovarian cancer mouse model [28]. Overexpression of miR-630 could also enhance HIF-3α expression, forming a positive feedback loop. Several reports have indicated models for how hypoxia-induced miRNAs regulates the switch between HIF-1a and HIF-3α in human endothelial cells [29], and their regulatory feedback circuit enhancing tumor metastasis in hepatocellular carcinoma [30]. We found HIF-3α binds to miR-630 promoter region and activates its expression. Meanwhile, miR-630 overexpression enhanced the expression level of HIF-3α, but repressed HIF-1α level. Given that HIF-3α and miR-630 were both consistently up-regulated by hypoxia, we proposed they may co-functionally regulate the cellular processes of HeLa cells under hypoxia.

Taken together, our results in this study firstly revealed the mechanisms of HIF-3α. We extensively investigated the cellular functions of HIF-3α-induced microRNA miR-630, and detected the HIF-3α/miR-630 positive loop to regulate multiple cellular processes. The underlying miR-630-mediated radioresistance can provide useful information for clinical consideration how to treat miR-630 mediated resistance to radiotherapy and hypoxia in the near future. The novel identified functions of HIF-3α and its regulatory loop with miR-630 in HeLa cells also provide theoretical basis for future clinical prognosis prediction and treatment of cervical cancer.

Abbreviations

ChIP
Chromatin immunoprecipitation
DEG
Differentially expressed gene
EMT
Epithelial-Mesenchymal Transition
HIF
Hypoxia-inducible factor

RT-qPCR
Reverse transcription quantitative polymerase chain reaction.

Declarations

Ethics approval and consent to participate

Not applicable.

Consent for publication

Not applicable.

Availability of data and materials

The datasets used and analysed during the current study are available from the corresponding author on reasonable request.

Competing interests

The authors declare no competing interests.

Funding

This study was financially supported founded by the Grant (no. 31770908 and no. 81272490) from National Natural Science Foundation of China.

Author Contributions

Qiaohui Gao and Junye Liu: Conceptualization; Qiaohui Gao, Zhenghua Ren, Shengyuan Jiao and Juan Guo: Methodology; Zhenghua Ren, Jin Wang and Xia Miao: Data curation; Shengyuan Jiao, Qiaohui Gao and Zhenghua Ren: Formal analysis; Qiaohui Gao, Zhenghua Ren, Shengyuan Jiao and Junye Liu: Roles/Writing – original draft and/or Writing – review & editing; Junye Liu: Supervision. All authors read and approved the final manuscript.

Acknowledgements

We would like to thank the ABLife group for their help in data analysis and discussion.

References

1. Global Burden of Disease Cancer C, Fitzmaurice C, Dicker D, Pain A, Hamavid H, Moradi-Lakeh M, MacIntyre MF, Allen C, Hansen G, Woodbrook R *et al*: **The Global Burden of Cancer 2013**. *JAMA Oncol* 2015, **1**(4):505-527.

2. Huang Z, Mayr NA, Yuh WT, Lo SS, Montebello JF, Grecula JC, Lu L, Li K, Zhang H, Gupta N *et al*: **Predicting outcomes in cervical cancer: a kinetic model of tumor regression during radiation therapy**. *Cancer Res* 2010, **70**(2):463-470.
3. Vaupel P: **Tumor microenvironmental physiology and its implications for radiation oncology**. *Semin Radiat Oncol* 2004, **14**(3):198-206.
4. Balamurugan K: **HIF-1 at the crossroads of hypoxia, inflammation, and cancer**. *Int J Cancer* 2016, **138**(5):1058-1066.
5. Zhou X, Guo X, Chen M, Xie C, Jiang J: **HIF-3alpha Promotes Metastatic Phenotypes in Pancreatic Cancer by Transcriptional Regulation of the RhoC-ROCK1 Signaling Pathway**. *Mol Cancer Res* 2018, **16**(1):124-134.
6. Kim J, Yao F, Xiao Z, Sun Y, Ma L: **MicroRNAs and metastasis: small RNAs play big roles**. *Cancer Metastasis Rev* 2018, **37**(1):5-15.
7. Jihang Yao BD, et al: **miR-27b is upregulated in cervical carcinogenesis and promotes cell growth and invasion by regulating CDH11 and epithelial-mesenchymal transition**. *Oncol Rep* 2016, **35(1)**: 1645-1651.
8. Zhang B, Chen J, Ren Z, Chen Y, Li J, Miao X, Song Y, Zhao T, Li Y, Shi Y *et al*: **A specific miRNA signature promotes radioresistance of human cervical cancer cells**. *Cancer Cell Int* 2013, **13**(1):118.
9. Song YF, Hong JF, Liu DL, Lin QA, Lan XP, Lai GX: **miR-630 targets LMO3 to regulate cell growth and metastasis in lung cancer**. *Am J Transl Res* 2015, **7**(7):1271-1279.
10. Kim D, Pertea G, Trapnell C, Pimentel H, Kelley R, Salzberg SJGb: **TopHat2: accurate alignment of transcriptomes in the presence of insertions, deletions and gene fusions**. 2013, **14**(4):R36.
11. Trapnell C, Williams BA, Pertea G, Mortazavi A, Kwan G, van Baren MJ, Salzberg SL, Wold BJ, Pachter L: **Transcript assembly and quantification by RNA-Seq reveals unannotated transcripts and isoform switching during cell differentiation**. *Nat Biotechnol* 2010, **28**(5):511-515.
12. M. D. Robinson DJM, G. K. Smyth: **edgeR: a Bioconductor package for differential expression analysis of digital gene expression data**. *Bioinformatics* 2010, **26**:139-140.
13. Xie C, Mao X, Huang J, Ding Y, Wu J, Dong S, Kong L, Gao G, Li CY, Wei L: **KOBAS 2.0: a web server for annotation and identification of enriched pathways and diseases**. *Nucleic Acids Res* 2011, **39**(Web Server issue):W316-322.
14. Nallamshetty S, Chan SY, Loscalzo J: **Hypoxia: a master regulator of microRNA biogenesis and activity**. *Free Radic Biol Med* 2013, **64**:20-30.
15. Masoud GN, Li W: **HIF-1alpha pathway: role, regulation and intervention for cancer therapy**. *Acta Pharm Sin B* 2015, **5**(5):378-389.
16. Zhang Y, Liu T, Meyer CA, Eeckhoute J, Johnson DS, Bernstein BE, Nussbaum C, Myers RM, Brown M, Li W *et al*: **Model-based Analysis of ChIP-Seq (MACS)**. *Genome biology* 2008, **9**(9):R137.
17. Shiloh Y, Ziv Y: **The ATM protein kinase: regulating the cellular response to genotoxic stress, and more**. *Nat Rev Mol Cell Biol* 2013, **14**(4):197-210.

18. Mees ST, Mardin WA, Wendel C, Baeumer N, Willscher E, Senninger N, Schleicher C, Colombo-Benkmann M, Haier J: **EP300--a miRNA-regulated metastasis suppressor gene in ductal adenocarcinomas of the pancreas**. *Int J Cancer* 2010, **126**(1):114-124.
19. Luo M, Ding L, Li Q, Yao H: **miR-668 enhances the radioresistance of human breast cancer cell by targeting IkappaBalpha**. *Breast Cancer* 2017, **24**(5):673-682.
20. Pedroza-Torres A, Campos-Parra AD, Millan-Catalan O, Loissell-Baltazar YA, Zamudio-Meza H, Cantu de Leon D, Montalvo-Esquivel G, Isla-Ortiz D, Herrera LA, Angeles-Zaragoza O *et al*: **MicroRNA-125 modulates radioresistance through targeting p21 in cervical cancer**. *Oncol Rep* 2018, **39**(3):1532-1540.
21. Gong XF, Yu AL, Tang J, Wang CL, He JR, Chen GQ, Zhao Q, He M, Zhou CX: **MicroRNA-630 inhibits breast cancer progression by directly targeting BMI1**. *Exp Cell Res* 2018, **362**(2):378-385.
22. Eoh KJ, Lee SH, Kim HJ, Lee JY, Kim S, Kim SW, Kim YT, Nam EJ: **MicroRNA-630 inhibitor sensitizes chemoresistant ovarian cancer to chemotherapy by enhancing apoptosis**. *Biochem Biophys Res Commun* 2018, **497**(2):513-520.
23. Yuan-Yuan Lyu F-MW, Xiao-Mei Yang, Can-Can Zhang, Fei Gu, Tian-Jiao Luo, Peng-Cheng Jiang, Rong Zhang: **MiR-630 acts as a tumor suppressor in cervical cancer and inhibits epithelial-mesenchymal transition in cervical cancer**. *Int J Clin Exp Pathol* 2017, **10**.
24. Farazi TA, Spitzer JI, Morozov P, Tuschl T: **miRNAs in human cancer**. *The Journal of pathology* 2011, **223**(2):102-115.
25. Schito L, Semenza GL: **Hypoxia-Inducible Factors: Master Regulators of Cancer Progression**. *Trends Cancer* 2016, **2**(12):758-770.
26. Yang SL, Wu C, Xiong ZF, Fang X: **Progress on hypoxia-inducible factor-3: Its structure, gene regulation and biological function (Review)**. *Mol Med Rep* 2015, **12**(2):2411-2416.
27. Zhang P, Yao Q, Lu L, Li Y, Chen PJ, Duan C: **Hypoxia-inducible factor 3 is an oxygen-dependent transcription activator and regulates a distinct transcriptional response to hypoxia**. *Cell Rep* 2014, **6**(6):1110-1121.
28. Rupaimoole R, Ivan C, Yang D, Gharpure KM, Wu SY, Pecot CV, Previs RA, Nagaraja AS, Armaiz-Pena GN, McGuire M *et al*: **Hypoxia-upregulated microRNA-630 targets Dicer, leading to increased tumor progression**. *Oncogene* 2016, **35**(33):4312-4320.
29. Janaszak-Jasiecka A, Bartoszewska S, Kochan K, Piotrowski A, Kalinowski L, Kamysz W, Ochocka RJ, Bartoszewski R, Collawn JF: **miR-429 regulates the transition between Hypoxia-Inducible Factor (HIF)1A and HIF3A expression in human endothelial cells**. *Sci Rep* 2016, **6**:22775.
30. Kai AK, Chan LK, Lo RC, Lee JM, Wong CC, Wong JC, Ng IO: **Down-regulation of TIMP2 by HIF-1alpha/miR-210/HIF-3alpha regulatory feedback circuit enhances cancer metastasis in hepatocellular carcinoma**. *Hepatology* 2016, **64**(2):473-487.

Figures

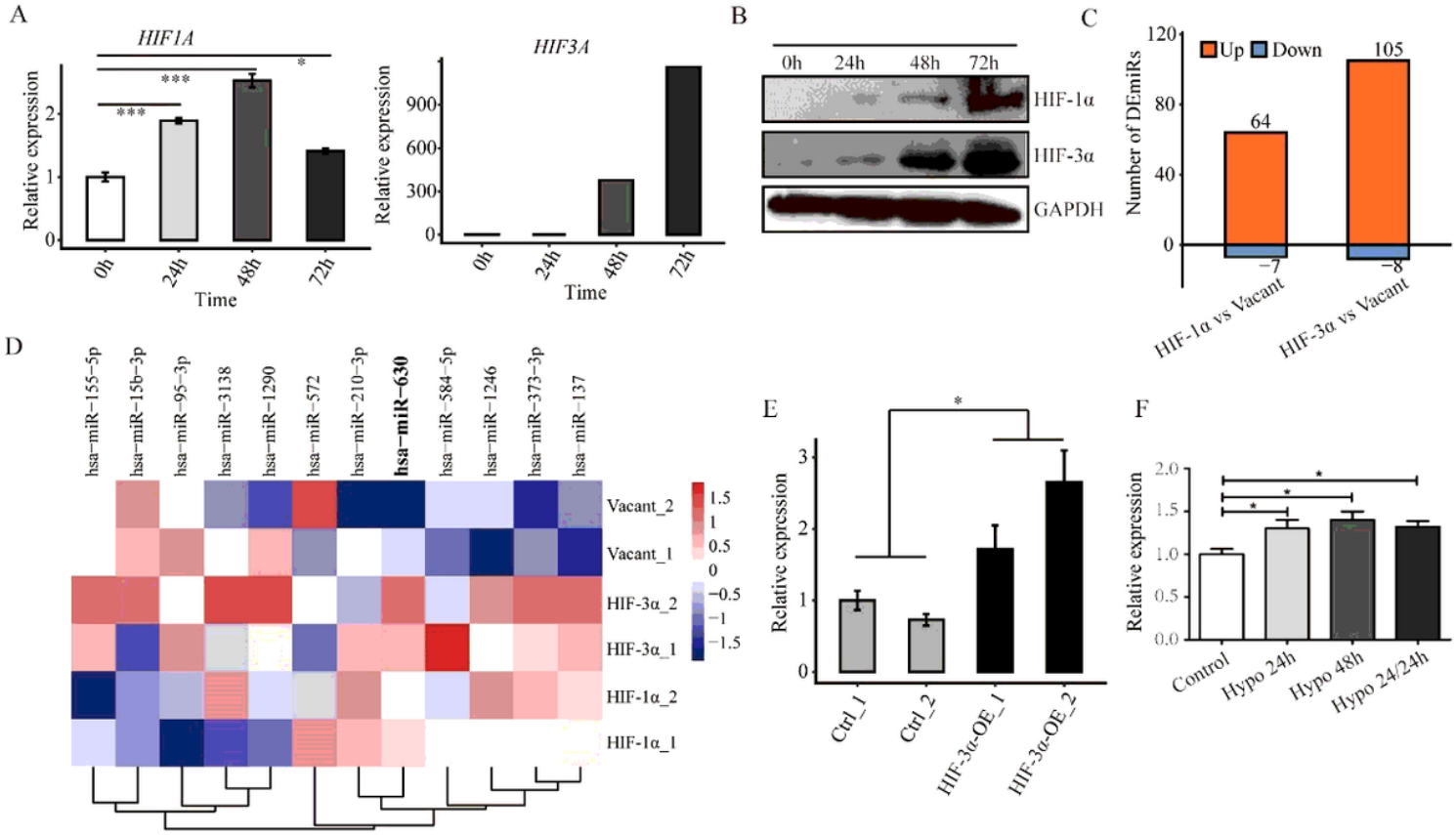

Figure 1

HIF-1A and HIF-3A promote miR-630 expression under hypoxia condition. (A) Bar plot showed the increased RNA level of HIF1A and HIF3A under hypoxia condition by RT-qPCR experiment. (B) Western blot result showed the increased protein level of HIF1A and HIF3A under hypoxia condition. (C) Bar plot showed the DEmiR number in HIF-1α vs vacant and HIF-3α vs vacant groups. (D) Hierarchical clustering heatmap showed the elevated expression level of selected miRNAs in HIF-1α and HIF-3α OE samples. (E) Bar plot showed the increased expression level of miR-630 under hypoxia condition by RT-qPCR experiment. (F) Bar plot showed the expression level of miR-630 under hypoxia condition by RT-qPCR experiment.

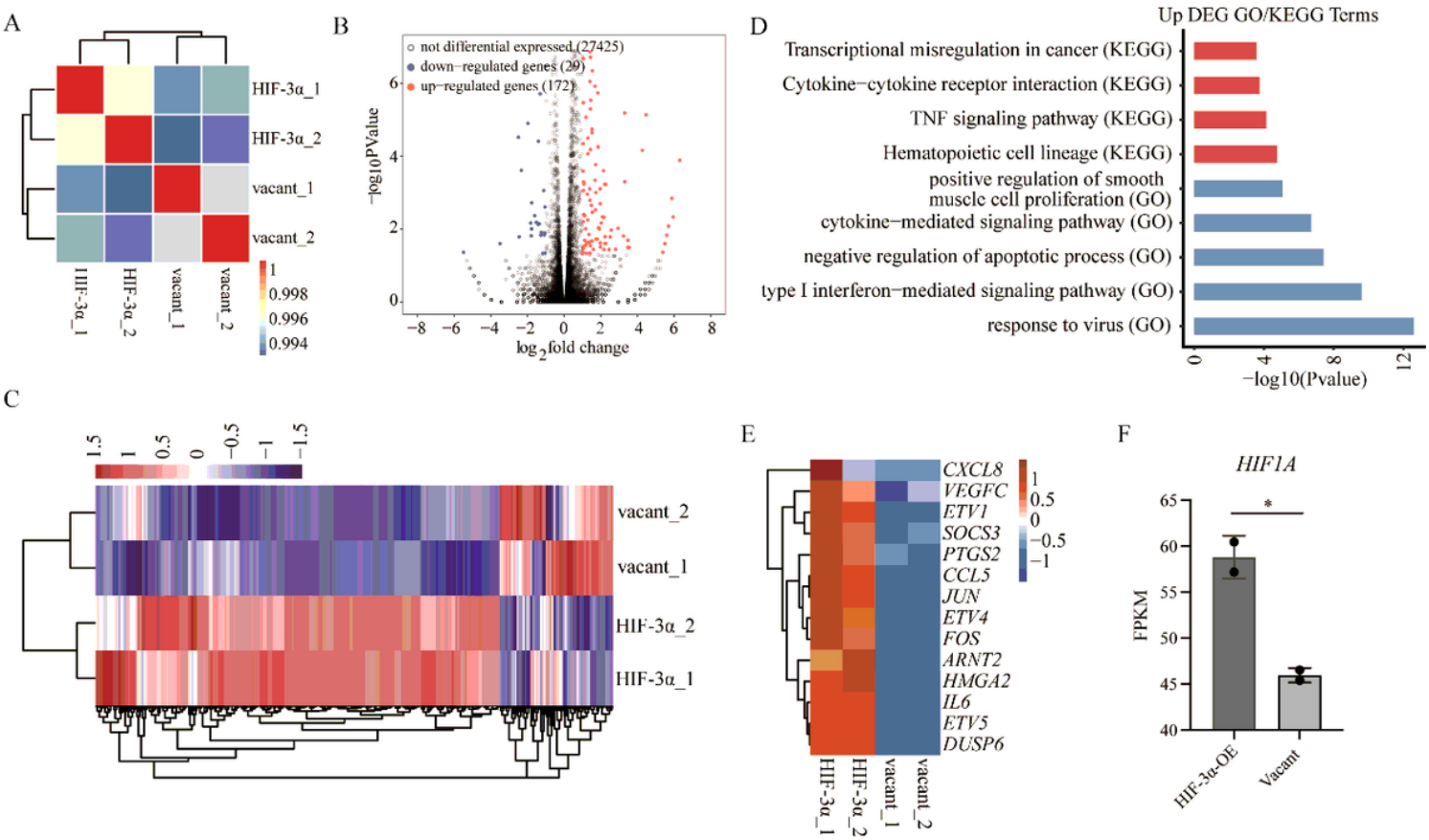

Figure 2

HIF-3α overexpression globally regulates gene expression in HeLa cells. (A) Sample correlation results showed clear separation between HIF-3α OE and vacant samples. (B) Volcano plot showed the DEGs results between HIF-3α OE and vacant samples. (C) Hierarchical clustering heatmap showed the dominant up-regulated genes after HIF-3α OE. (D) Top functional enriched GO BP terms and KEGG pathways for HIF-3α up-regulated genes. (E) Heat map showed the up-regulated genes by HIF-3α OE. (F) Bar plot showed the expression level of HIF1A transcripts under HIF3A overexpression and repression conditions.

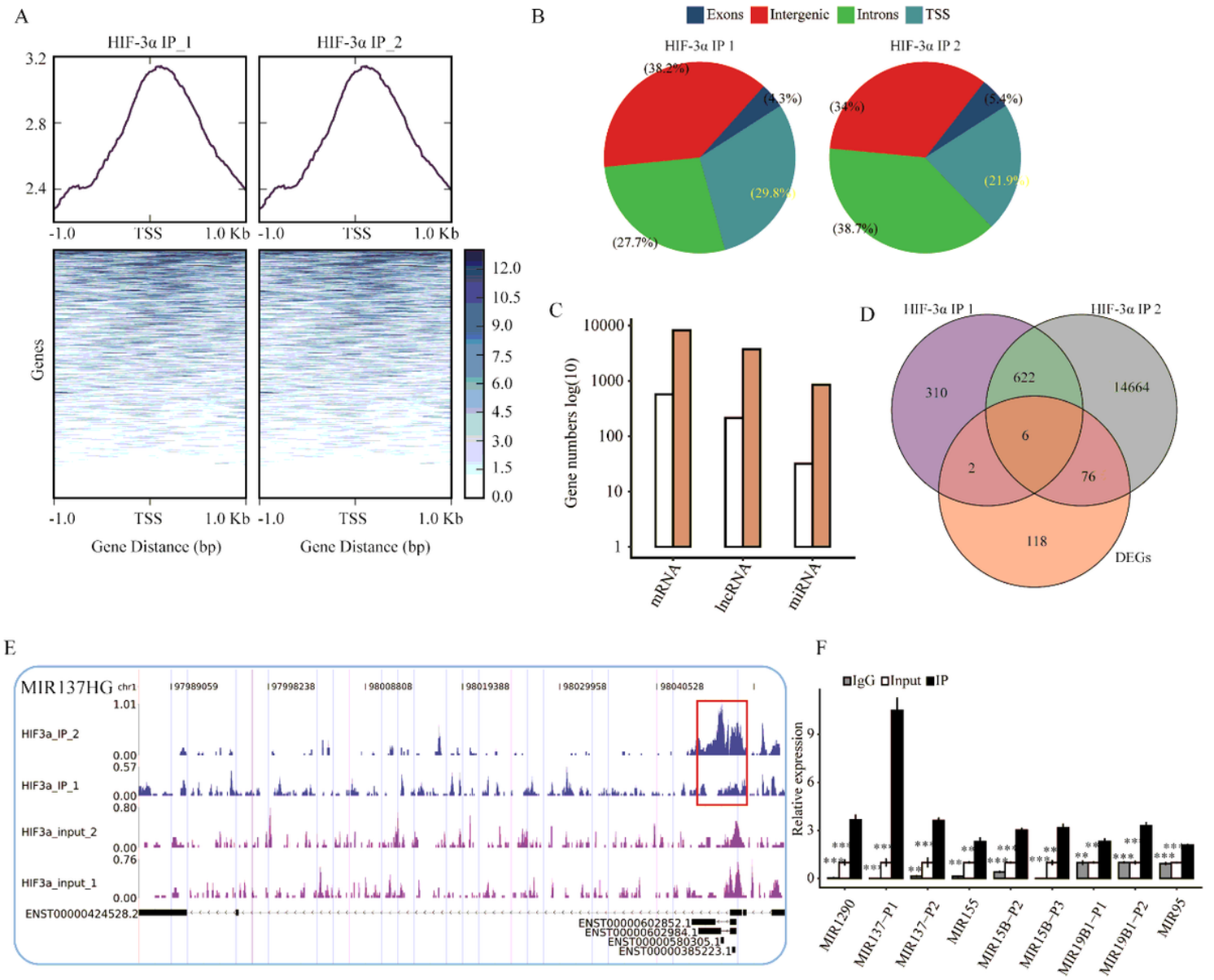

Figure 3

ChIP-seq results of HIF-3α showed it binding preference at promoter region. (A) Reads density heatmap plot showed the enriched reads distribution around gene TSS sites. (B) Pie chart showed the percentage of peaks from four genomic regions. (C) Barplot showed the percentage of bound genes classified by their coding types. The white and brown bars represented two biological replicates of HIF-3α ChIP-seq data. (D) Venn diagram showed HIF-3α bound genes and HIF-3α-regulated DEGs. (E) Reads distribution of bound miRNAs miR-137. Red rectangle represents the bound region of HIF-3α. (F) Bar plot showed the validation results of ChIP-qPCR experiments.

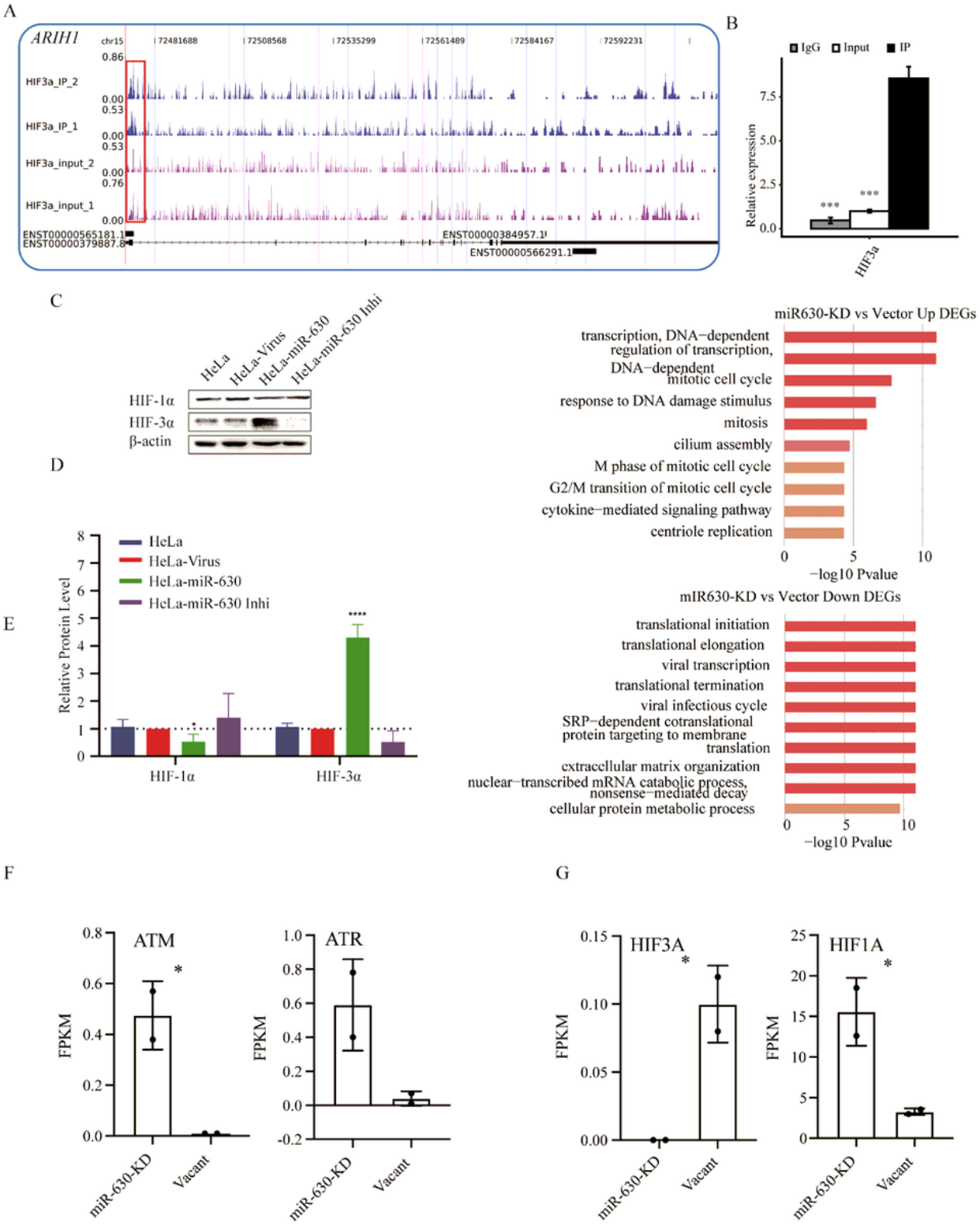

Figure 4

RNA-seq revealed the functions of miR-630 targets in HeLa cells. (A) Reads distribution plot showed the significant HIF3A binding density on the promoter of miR-630 host gene. Red frame represented the HIF3A binding peak. (B) Bar plot showed the ChIP-qPCR results of the HIF-3a binding density on the promoter of miR-630 host gene. (C) Western blot showed the expression change of HIF1A and HIF3A under miR-630 overexpression and knockdown conditions. (D) Bar plot showed the quantified level of WB

result showed in (C). Three biological replicates were included in this panel. (E) Bar plot showed the enriched GP BP terms for up-regulated genes (left) and down-regulated genes (right) by miR-630 inhibition. (F) Bar plot showed the increased expression level of ATM and ATR by miR-630 inhibition. (G) Bar plot showed the increased expression level of HIF1A and decreased expression level of HIF3A by miR-630 inhibition.

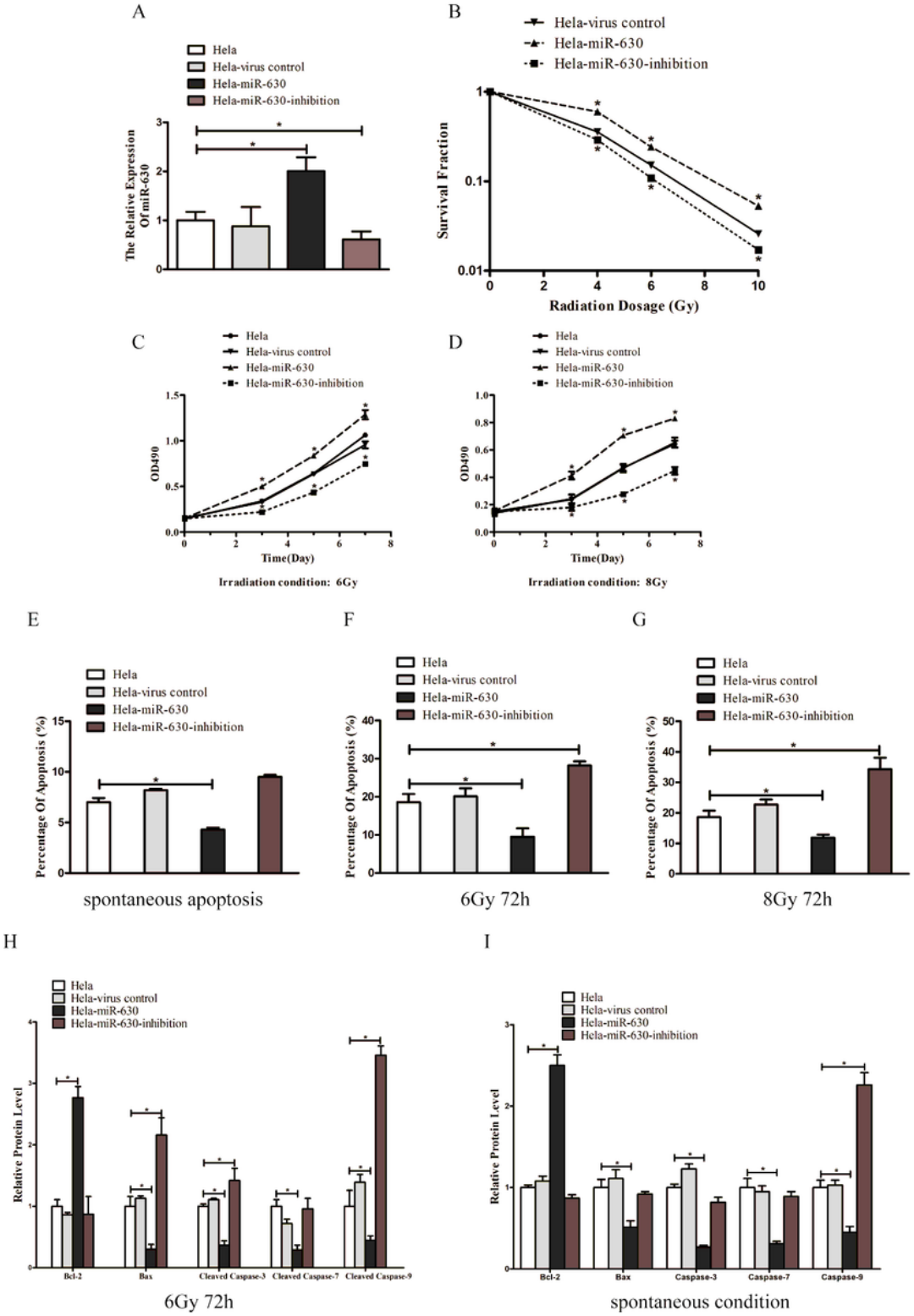

Figure 5

MiR-630 increases the radioresistance and significantly reduce the apoptosis level of HeLa cells under spontaneous and radiation-treated conditions. (A) RT-qPCR analysis of lentiviral overexpression of miR-630 and inhibition in HeLa cell lines. (B) Colony formation assay showing the higher radioresistance by miR-630 overexpression and opposite phenotype by miR-630 inhibitor. * $p < 0.05$. (C-D) Overexpression of miR-630 increased the cell proliferation rates of HeLa cells under irradiation conditions. (E) MiR-630 overexpression reduced the spontaneous apoptosis level of HeLa cells. (F-G) MiR-630 overexpression reduced the radiation-induced apoptosis level of HeLa cells. (H) Western blotting showing the expression change of several apoptosis markers in HeLa cells with miR-630 overexpression or inhibition under radiation-treated condition. (I) Western blotting showing the expression change of several apoptosis markers in HeLa cells with miR-630 overexpression or inhibition under spontaneous condition.

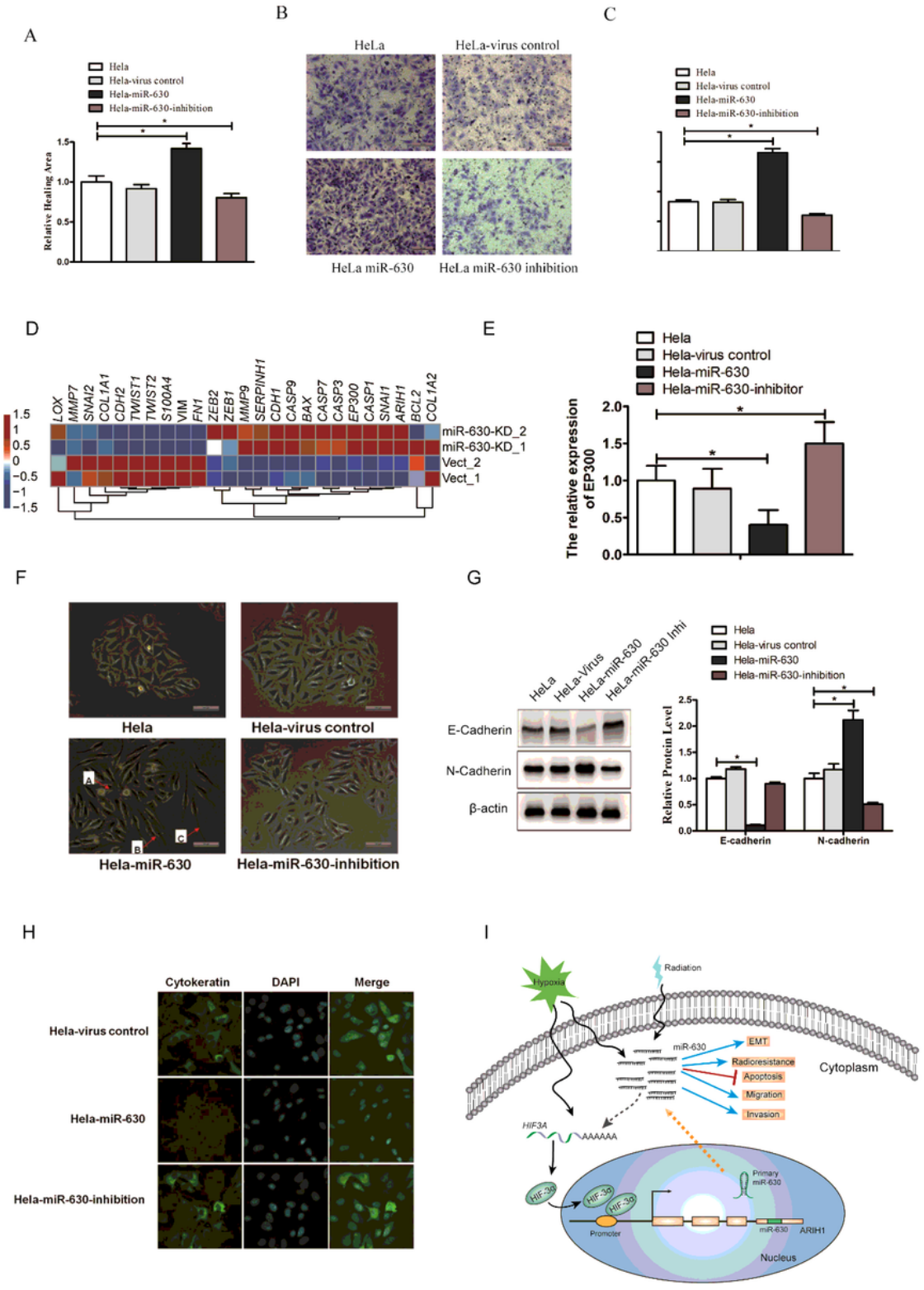

Figure 6

Effects of miR-630 on migration and invasion of HeLa cell line and MiR-630 promoted HeLa metastasis is mediated by the EMT. (A) Wound healing assay was performed to compare the migratory capabilities of HeLa、HeLa-virus control and HeLa-miR-630-inhibitor cell. *P<0.05. The graph is the quantification of migration rates analyzed in HeLa、HeLa-virus control、HeLa-miR-630 and HeLa-miR-630-inhibitor cell respectively. (B-C) Representative invasion images of HeLa、HeLa-virus control、HeLa-miR-630 and HeLa-

miR-630-inhibitor cell by transwell invasion assay. The right graph is the quantification of invasion number analyzed in four cells. (D)Heat map plot showed the expression level change of miR-630 targets that are transcription factors related to EMT. (E)Bar plot showed the RT-qPCR results of transcription factor EP300 under miR-630 overexpression and knockdown conditions. (F)The morphology of HeLa, HeLa-virus control, HeLa-miR-630 and HeLa-miR-630-inhibition cells. Note: (A) Cell space became wide; (B) Spindle-cell morphology formed; (C) Pseudopodia were stretched out. Scale bar = 100) (G) WB was performed to analysis EMT maker expression. (H) Cellular staining showed the cytokeratin distribution in the HeLa cells. (I) Working model showed the HIF3A-miR-630 regulatory loop in HeLa cells.

Supplementary Files

This is a list of supplementary files associated with this preprint. Click to download.

- SupplementalFigures.docx
- SupplementalTables.pdf